Nanoscale Res Lett (2009) 4:1257–1262
DOI 10.1007/s11671-009-9389-4

NANO EXPRESS

Structural Characterization of Mesoporous Silica Nanofibers Synthesized Within Porous Alumina Membranes

Zhihong Gong · Guangbin Ji · Mingbo Zheng · Xiaofeng Chang · Weijie Dai · Lijia Pan · Yi Shi · Youdou Zheng

Received: 29 May 2009 / Accepted: 3 July 2009 / Published online: 14 July 2009
© to the authors 2009

Abstract Mesoporous silica nanofibers were synthesized within the pores of the anodic aluminum oxide template using a simple sol–gel method. Transmission electron microscopy investigation indicated that the concentration of the structure-directing agent ($EO_{20}PO_{70}EO_{20}$) had a significant impact on the mesostructure of mesoporous silica nanofibers. Samples with alignment of nanochannels along the axis of mesoporous silica nanofibers could be formed under the P123 concentration of 0.15 mg/mL. When the P123 concentration increased to 0.3 mg/mL, samples with a circular lamellar mesostructure could be obtained. The mechanism for the effect of the P123 concentration on the mesostructure of mesoporous silica nanofibres was proposed and discussed.

Keywords Mesoporous silica · Nanofiber · Anodic aluminum oxide · P123 · Template synthesis

Introduction

Mesoporous materials with ordered nanochannels, tunable pore size from 2 to 50 nm, large surface area, and high hydrothermal and thermal stability have rapidly sprang up since 1990s [1, 2]. Numerous research works about mesoporous materials have been reported, such as SiO_2 [3, 4], TiO_2 [5, 6], carbon [7, 8], NiO [9, 10], and ZnO [11, 12]. Among these materials, mesoporous silica is widespread due to their ultrafine nanograin, highly efficient catalysis and separation [13–15]. With the development of nanotechnology, it is expected to synthesize 1-Dimensional (1D) mesoporous silica with orderly arranged and vertical nanochannel structure because of their potential applications such as waveguides [16], lasers [17], and templates that are used to grow functionalized ultrafine nanowire arrays [18, 19]. Among the different preparation procedures, the template method was widely adopted [20, 21]. Compared with other templates, porous anodic aluminum oxide (AAO) membranes have orderly arranged and vertical 1D channel structure. Previously, several research groups have synthesized mesoporous silica nanofibers (MSNFs) within the pores of the AAO templates [22–29].

Different mesostructures of MSNFs, such as a circular hexagonal column, a circular lamellar cylinder, and a parallel hexagonal column, have been synthesized by the different preparation procedures. It is difficult to obtain the desired mesostructures for MSNFs within the AAO templates. Because several parameters, such as the size of the AAO template nanochannels, the surfactant, the hydrophilicity/hydrophobicity of the channel wall, and the precursor compositions, play key roles in the formation of the pore size, the orientation, and the morphology of MSNFs. Wu et al. [18] synthesized MSNFs with chiral mesopores such as single and double helical geometries inside the AAO membranes. Different mesostructures of MSNFs were obtained by controlling the pore size of AAO membranes. Yamaguchi et al. prepared MSNFs with 1D, 3D, and the mixture of 1D and 3D alignments of the silica-nanochannels. They reported that the mesostructure of MSNFs could be tuned by experimental conditions (aging

Z. Gong · G. Ji (✉) · M. Zheng · X. Chang · W. Dai
Nanomaterials Research Institute, College of Material Science and Technology, Nanjing University of Aeronautics and Astronautics, 210016 Nanjing, People's Republic of China
e-mail: gbji@nuaa.edu.cn

G. Ji · L. Pan · Y. Shi · Y. Zheng
National Laboratory of Solid State Microstructure and Department of Physics, Nanjing University, 210093 Nanjing, People's Republic of China

time and temperature) for preparing the precursor solution [30]. Wang et al. found that the mesostructure of MSNFs was sensitive to the AAO template structure and aging conditions [31]. Platschek et al. [32] systematically investigated the effect of interfacial interactions and inorganic salt addition upon the orientation of MSNFs nanochannels. MSNFs with a 2D columnar hexagonal structure, a 2D circular hexagonal structure, and a mixture of 2D columnar and circular hexagonal structure were obtained by using different surfactants. However, to the best of our knowledge, a systematic study of the effect of the concentration of surfactant on the mesostructure of MSNFs in the confined space of the AAO nanochannels is rare.

Herein, we report a simple sol–gel method to synthesize MSNFs within the AAO templates. It is found that the mesostructure of MSNFs in the confined space of the AAO nanochannel was influenced by the concentration (varied from 0.1 to 0.4 mg/mL) of the P123 surfactant.

Experimental Section

Synthesis

The commercially available AAO membranes (Whatman, Anodisc 47) with a nominal pore diameter of 250 nm and 60 μm thickness were used as templates. The surfactant poly (ethylene oxide)-b-poly (propylene oxide)-b-poly (ethylene oxide) block copolymer $EO_{20}PO_{70}EO_{20}$ (Pluronic P123) was purchased from Sigma–Aldrich. The precursor solution was prepared according to the literature [33] with some modifications. Firstly, a mixture of P123 (0.4–1.6 g) and ethanol solution (40 mL) was stirred at room temperature until the P123 surfactant has dissolved completely in ethanol. Secondly, tetraethyl orthosilicate (TEOS: 0.93 g) was added to the mixture solution. The resultant mixture solution was continued to stir at room temperature for 10 min. The precursor solution was obtained after adding 0.4 g of hydrochloric acid (38%) to the P123/TEOS mixture solution and stirring at room temperature for 10 min. Then, the AAO template was added into the precursor solution at room temperature. After the ethanol vaporized completely, the AAO membrane was taken out from the sol, and the residual sol on the surface was completely scratched away. Then, the AAO template including the precursor was dried at 60 °C for 12 h in air. A calcination process was carried out at 400 °C in air for 3 h with a heating rate of 1 °C/min. The as-prepared MSNFs using 0.1, 0.15, 0.2, 0.225, 0.3, 0.35, and 0.4 mg/mL of P123 in the precursor solution were denoted as MSNFs-1, MSNFs-2, MSNFs-3, MSNFs-4, MSNFs-5, MSNFs-6, and MSNFs-7, respectively. The AAO template including MSNFs was denoted as AAO/MSNFs.

Characterization

The morphology of MSNFs was observed by field emission scanning electron microscope (FE-SEM, JEOL S4800 and Gemini LEO 1530) with attached energy dispersive spectrometry (EDS) and transmission electron microscope (TEM, JEOL JEM 2100). For the SEM measurement, a small piece of AAO/MSNFs was slightly etched by immersing into an aqueous solution of 7 wt% H_3PO_4 for 12 h to obtain a clear top view. Meanwhile, in order to observe the MSNFs formed inside the pore of AAO membrane, the AAO/MSNFSs was immersed into an aqueous solution of 7 wt% H_3PO_4 for 4 days at room temperature for removing the AAO membrane completely. Then, the samples were washed with distilled water for several times. For the TEM investigation, the AAO/MSNFs were immersed into an aqueous solution of 7 wt% H_3PO_4 for 4 days at room temperature and dispersed in absolute ethanol; then, a small drop of solution was placed on Cu grids covered with carbon film. N_2 adsorption–desorption analysis was measured on a Micrometrics ASAP2010 instrument.

Results and Discussion

The Morphology Characterization of the MSNFs

SEM observation was used to characterize the morphology feature of the as-prepared MSNFs. The top-view SEM image (see Fig. 1a) of the sample clearly shows that most of the pores of AAO membranes are filled with MSNFs. Also, we observed the spaces between MSNFs and the walls of the pores of AAO membrane due to the contraction under the drying and calcination processes, which corresponds to the previous report [31]. Figure 1b, c, and d shows the bundle-shaped MSNFs after removal of the AAO membrane. The average diameter of each MSNFs is about 200 nm, which mainly depends on the pore size of the AAO membrane.

TEM characterization was employed to further investigate the inner structure of MSNFs. Figure 2 shows TEM images of MSNFs prepared by using different concentrations of P123 (varied from 0.1 to 0.4 mg/mL) in the precursor solution. It is found that the inner structures of MSNFs-1, MSNFs-3, and MSNFs-7 (given in Fig. 2a, d, and i) are complicated. Fig. 2b and c shows that 1D alignment of the silica-nanochannels with the orientation of nanochannels along the long axis of the nanopores of the AAO template under the P123 concentration of 0.15 mg/mL (MSNFs-2). The average diameter of nanopores is estimated in the range of 6–7 nm. With the concentration of P123 increasing to 0.225 mg/mL (MSNFs-4),

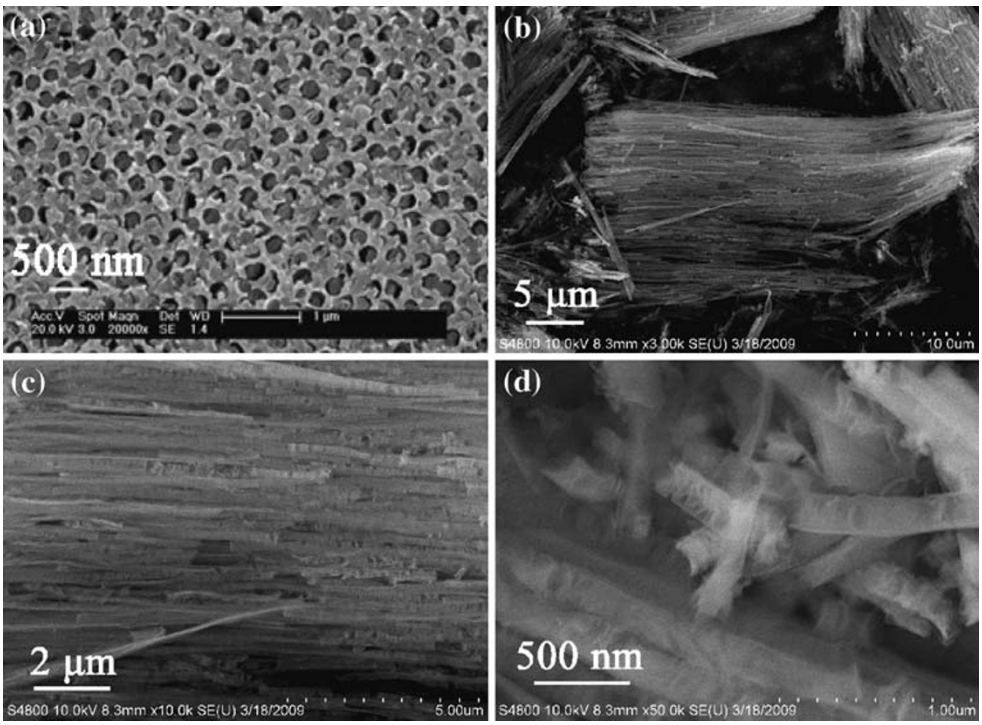

Fig. 1 **a** Top-view SEM image of AAO/MSNFs membranes and **b–d** side view SEM images of MSNFs

the sample with a circular lamellar mesostructure symmetrically along the edges and a circular columnar mesostructure in the central region is observed in Fig. 2e. This mesostructure attributes to the confined growth of the circular columnar mesostructure inside the pores of the AAO membrane, and it is made up of a circular multilayered lamellar mesostructure filled around the AAO nanochannel. When the concentration of P123 increase to 0.3 or 0.35 mg/mL, only a circular lamellar mesostructure can be found due to the formation of the circular columnar mesostructure is suppressed (Fig. 2f, g, and h). Obviously, the silica circular layers are coaxially oriented within MSNFs. The layer-to-layer distance is estimated around 30–50 nm. Figure 2e and g indicate that the mesostructure of MSNFSs-4 is a transitional structure from a circular columnar mesostructure to a circular lamellar mesostructure. The TEM results clearly indicate that the mesostructure of MSNFs can significantly be affected by the concentration of P123 in the precursor solution. The schematic illustration in Fig. 3 describes the inner structural transformation of MSNFs with the varying the concentrations of P123 (0.15, 0.225, and 0.3 mg/mL). Although the complicated mesostructures of MSNFs in Fig. 2a, d, and i were not described in the schematic illustration because of their complicated structures, these complicated mesostructures indicated that the mesostructure of MSNFs was changed by varying the concentration of P123. Under the confined space of the AAO nanochannels, three representative mesostructures for MSNFs were obtained by varying the concentration of P123. When the concentration of P123 was 0.15 mg/mL, MSNFs-2 was composed of columned nanochannels (Fig. 3a). The orientation of nanochannels paralleled the long axis of the AAO nanochannel. With the concentration of P123 increasing to 0.225 mg/mL, two types of mesostructures formed in MSNFs-4 (Fig. 3b). These were the columned mesopores with the orientation of nanochannel circling the axis of the AAO nanochannels and the concentric multilayered lamellar mesostructure. MSNFs-5 with the concentric multilayered lamellar mesostructure formed, when the concentration of P123 increased to 0.3 mg/mL (Fig. 3c).

It is well known that the shape of the micelles formed in the aqueous solutions dramatically depends on the concentration and the temperature. The relationship of the concentration with the structure has been investigated widely by dynamic light scattering (DLS), pulsed-field-gradient NMR, and so forth [34–40]. Take the typical triblock copolymer (P123) for an example, various morphologies of the micelles, such as spherical, cylindrical, and lamellar, can be obtained by using different concentrations of the surfactant (P123), because of the hydrophobic and hydrophilic interaction between the inner and outer region in a micelle. Wanka et al. [41] studied the phase diagrams and aggregation behavior of poly (oxyethylene)-poly (oxypropylene)–poly (oxyethylene) triblock copolymers in aqueous solution. They found that block copolymers exhibit a rich variety of

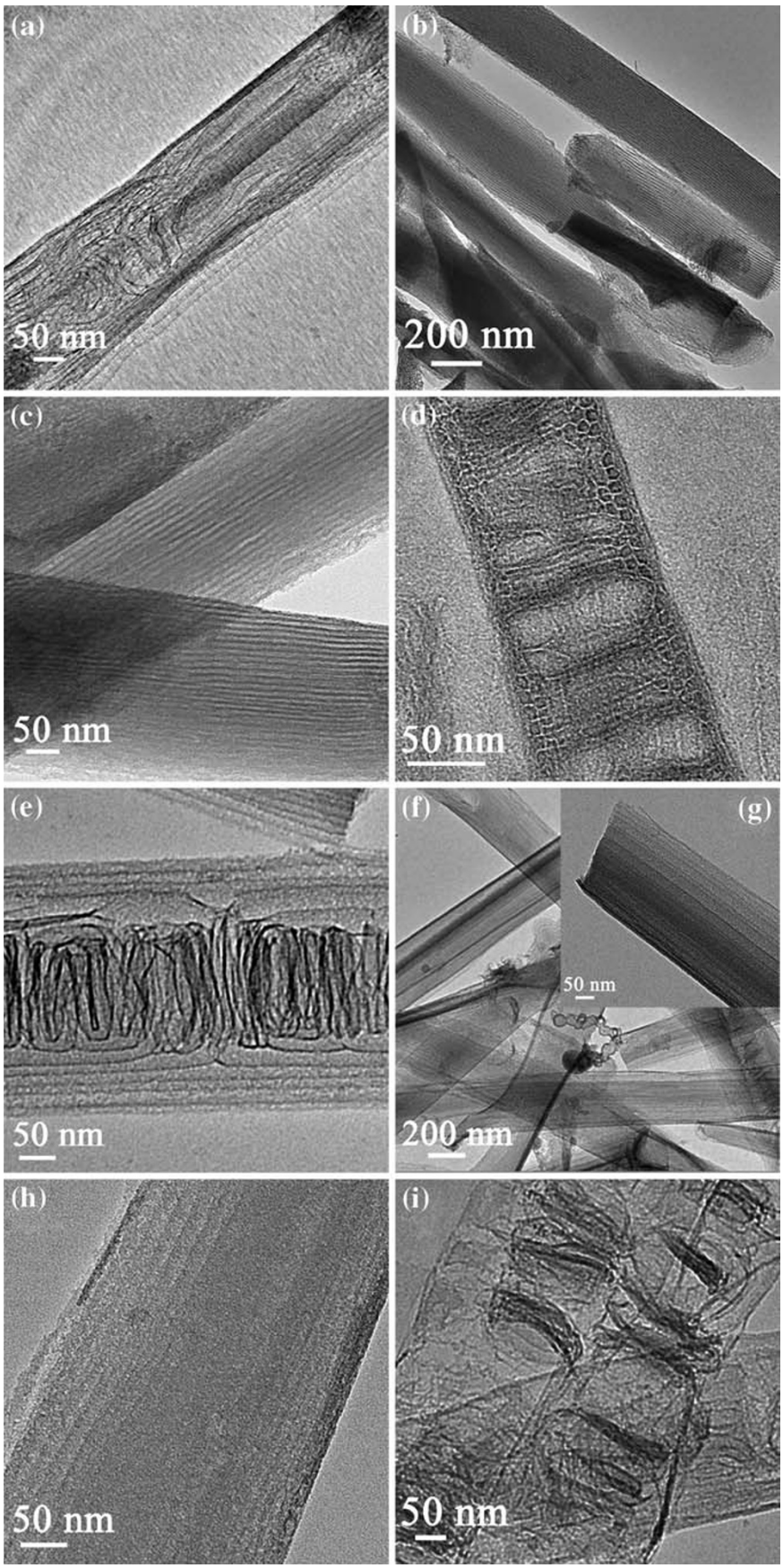

Fig. 2 TEM images of the MSNFs samples: **a** MSNFs-1; **b**, **c** MSNFs-2; **d** MSNFs-3; **e** MSNFs-4; **f**, **g** MSNFs-5; **h** MSNFs-6; and **i** MSNFs-7

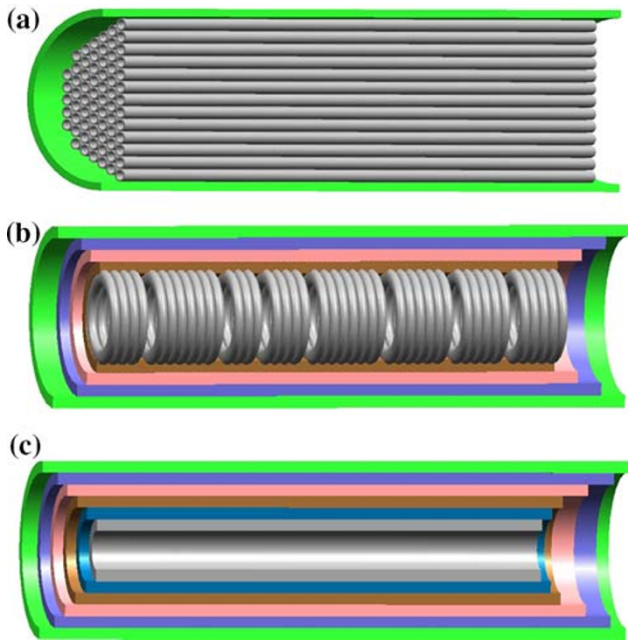

Fig. 3 Schematic diagrams concerning the change in the mesostructure of MSNFs with increasing the concentrations of P123: (**a**) 0.15 mg/mL; (**b**) 0.225 mg/mL; and (**c**) 0.3 mg/mL

equilibrium symmetries (spherical, cylindrical, and lamellar) that could be controlled by varying the concentration and the temperature.

Meanwhile, the confinement effects are also important to the morphology of a micelle. Stucky et al. [18] reported that in a physically confined environment, interfacial interactions, symmetry breaking, structural frustration, and confinement-induced entropy loss could play dominant roles in determining molecular organization.

In this present work, several complicated mesostructures displayed in Fig. 2a, d, and i have been observed. Although the mechanism was not very clear, it is considered that these results could possibly be ascribed by the effects of both the concentration of surfactant and the confined space, because of the fact that some simple mesostructures, such as the mixture of cylindrical and lamellar, the alignment of nanochannels, and the circular lamellar, have been fabricated by using different amount of P123 in ethanol solution, and the results are in agreement with the previous reported [30, 31, 33]. Thus, we propose that the phase of the surfactant (P123) micelles has significant impact on the mesostructure of MSNFs in the confined space of the AAO

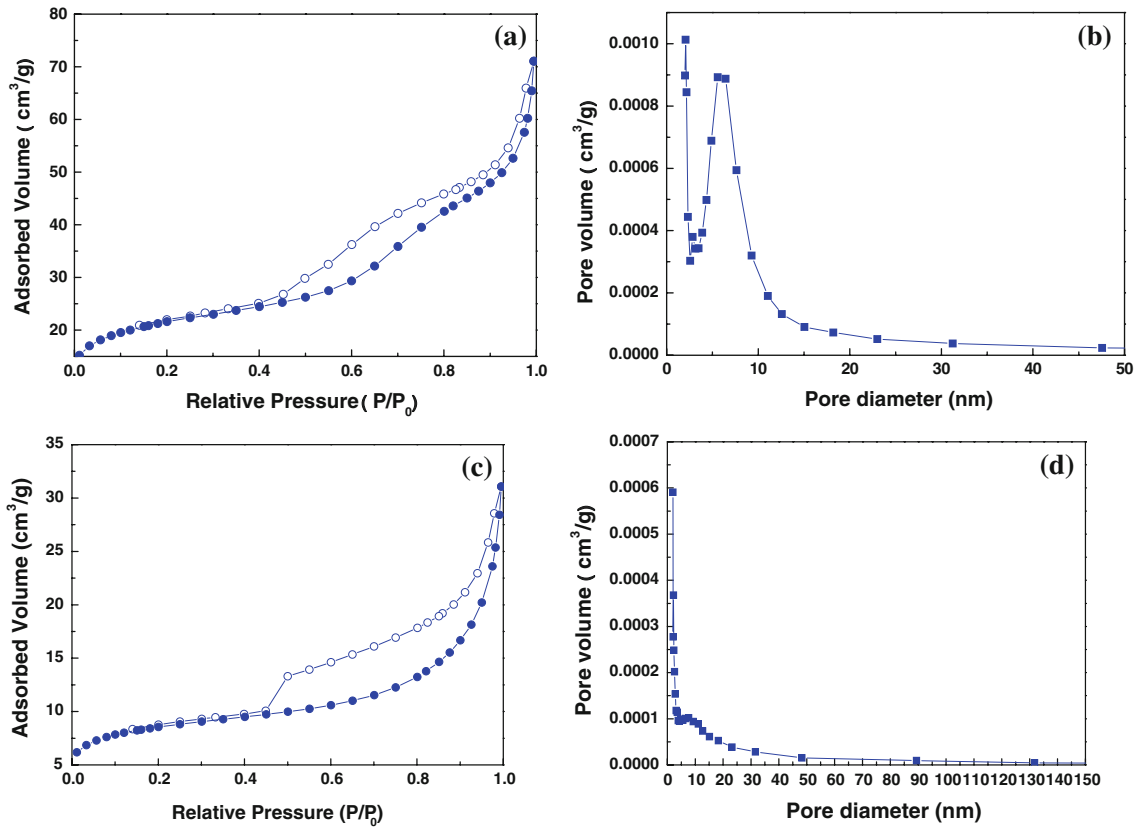

Fig. 4 N_2 adsorption–desorption isotherms and BJH pore-size distribution plots of the samples: **a**, **b** AAO/MSNFs-2 and **c**, **d** AAO/MSNFs-5

nanochannel under the same others experimentation condition.

N_2 Adsorption–Desorption Isotherms Analysis

Figure 4 shows the N_2 adsorption–desorption isotherms and the pore-size distribution curves for AAO/MSNFs-2 and AAO/MSNFs-5, respectively. Figure 4a and c shows the type IV with type H4 hysteresis loops, which are typical for mesoporous materials. There are dissimilarities for the two N_2 adsorption–desorption isotherms, which is possibly due to the different nanochannel structure of MSNFs. Figure 4b and d shows the pore-size distribution curves of AAO/MSNFs-2 and AAO/MSNFs-5, which are in agreement with the results of TEM analysis. From the distribution curves, the sample AAO/MSNFs-2 has a narrow distribution in the range of 5–10 nm (Fig. 4b). For the sample AAO/MSNFs-2, a broad pore-size distribution is observed (Fig. 4d). Meanwhile, the pore volumes for AAO/MSNFs-2 and AAO/MSNFs-5 are estimated to be 0.110 and 0.048 cm^3/g, respectively. The Brunauer–Emmett–Teller (BET) surface area for AAO/MSNFs-2 and AAO/MSNFs-5 are estimated to be 73.0 and 28.7 m^2/g, respectively.

Conclusions

In summary, MSNFs have been prepared within the pores of the AAO templates using a simple sol–gel method. At the same time, we found that MSNFs with alignment of the silica-nanochannels, a circular lamellar cylinder and other complicated mesostructures could be regulated by controlling the concentration of P123 in the precursor solution. It is considered that the phase of P123 micelles has a significant impact on the mesostructure of MSNFs in the confined space of the AAO nanochannels. The extensive structural control achieved for the mesoporous silica has a potential application to a wide variety of fields such as catalysis, adsorption, separation, nanoelectronic, and nanooptic.

Acknowledgments Financial support from the National Natural Science Foundation of China (50701024), National Key Project of Fundamental Research (973, No. 2007CB936300), China Postdoctoral Science Foundation (20080430164 and 200801366), and Jiangsu Postdoctoral Science Foundation (0801040B) are gratefully acknowledged.

References

1. D.Y. Zhao, J.L. Feng, Q.S. Huo, B. Melose, G.H. Fredrickson, B.F. Chmelka, G.D. Stucky, Science **279**, 548 (1998)
2. D.Y. Zhao, Q.S. Huo, J.L. Feng, B.F. Chmelka, G.D. Stucky, J. Am. Chem. Soc. **120**, 6024 (1998)
3. H.R. Byon, B. Chung, T. Chang, H.C. Choi, Chem. Mater. **20**, 6600 (2008)
4. E. Bloch, P.L. Llewellyn, T. Phan, D. Bertin, V. Hornebecq, Chem. Mater. **21**, 48 (2009)
5. I. Bannat, K. Wessels, T. Oekermann, J. Rathousky, D. Bahnemann, M. Wark, Chem. Mater. **21**, 1645 (2009)
6. M.C. Tsai, J.C. Chang, H.S. Sheu, H.T. Chiu, C.H. Lee, Chem. Mater. **21**, 499 (2009)
7. C. Song, J.P. Du, J.H. Zhao, S. Feng, G.X. Du, Z.P. Zhu, Chem. Mater. **21**, 1524 (2009)
8. A. Stein, Z.Y. Wang, M.A. Fierke, Adv. Mater **21**, 265 (2009)
9. W. Yue, W.Z. Zhou, Chem. Mater. **19**, 2359 (2007)
10. J.R.A. Sietsma, J.D. Meeldijk, M. Versluijs-Helder, A. Broersma, A. Jos van Dillen, P.E. de Jongh, K.P. de Jong, Chem. Mater. **20**, 2921 (2008)
11. D. Chandra, S. Mridha, D. Basak and A. Bhaumik, Chem. Commun., 2384 (2009)
12. Y.Y. Song, X.B. Cao, Y. Guo, P. Chen, Q.R. Zhao, G.Z. Shen, Chem. Mater. **21**, 68 (2009)
13. Y.J. Han, J.M. Kim, G.D. Stucky, Chem. Mater. **12**, 2068 (2000)
14. J. Lee, J.C. Park, H. Song, Adv. Mater. **20**, 1532 (2008)
15. J. W. Zhao, F. Gao, Y. L. Fu, W. Jin, P. G. Yang, D. Y. Zhao, Chem. Commun., 752 (2002)
16. Q.S. Huo, D.Y. Zhao, J.L. Feng, K. Weston, S.K. Buratto, G.D. Stucky, S. Schacht, F. Schueth, Adv. Mater. **9**, 974 (1997)
17. J. Loerke, F. Marlow, Adv. Mater. **14**, 1745 (2002)
18. Y.Y. Wu, G.S. Cheng, K. Katsov, S.W. Sides, J.F. Wang, J. Tang, G.H. Fredrickson, M. Moskovits, G.D. Stucky, Nature Mater. **3**, 816 (2004)
19. Y.Y. Wu, T. Livnch, Y.X. Zhang, G.S. Cheng, J.F. Wang, J. Tang, M. Moskovits, G.D. Stucky, Nano Lett. **4**, 2337 (2004)
20. M. Steinhart, J.H. Wendorff, A. Greiner, R.B. Wehrspohn, K. Nielsch, J. Schilling, J. Choi, U. Gosele, Science **296**, 1997 (2002)
21. C.P. Li, B.K. Teo, X.H. Sun, N.B. Wong, S.T. Lee, Chem. Mater. **17**, 5780 (2005)
22. Z.L. Yang, Z.W. Niu, X.Y. Gao, Z.Z. Yang, Y.F. Lu, Z.B. Hu, C.C. Han, Angew. Chem. Int. Ed. **42**, 4201 (2003)
23. Q.Y. Lu, F. Gao, S. Komarneni, T.E. Mallouk, J. Am. Chem. Soc. **126**, 8650 (2004)
24. G. Kickelbick, Small **1**, 168 (2005)
25. W.S. Chae, S.W. Lee, Y.R. Kim, Chem. Mater. **17**, 3072 (2005)
26. B. Platschek, N. Petkov, T. Bein, Angew. Chem. Int. Ed. **45**, 1134 (2006)
27. S. Yoo, M.D. David, D.F. Shantz, Langmuir **22**, 1839 (2006)
28. N. Petkov, B. Platschek, M.A. Morris, J.D. Holmes, T. Bein, Chem. Mater. **19**, 1376 (2007)
29. V. Cauda, L. Muhlstein, B. Onida, T. Bein, Micro. Meso. Mater. **118**, 435 (2009)
30. A. Yamaguchi, H. Kaneda, W. Fu, N. Teramae, Adv. Mater. **20**, 1034 (2008)
31. K. Jin, B.D. Yao, N. Wang, Chem. Phys. Lett. **409**, 172 (2005)
32. B. Platschek, N. Petkov, D. Himsl, S. Zimdars, Z. Li, R. Köhn, T. Bein, J. Am. Chem. Soc. **51**, 17362 (2008)
33. D.H. Wang, R. Kou, Z.L. Yang, J.B. He, Z.Z. Yang, Y.F. Lu, Chem. Commun. **2**, 166 (2005)
34. P. Alexandridis, T. Alan Hatton, Colloids Surf. A: Physicochem. Eng. Asp. **96**, 1 (1995)
35. Z. Zhou, B. Chu, J. Colloid Interface Sci. **126**, 171 (1988)
36. P. Mukerjee, K.J. Mysels, *Critical micelle concentrations of aqueous surfactant systems, NSRDS-NBS 36* (Government Printing Office, Washington, DC, 1971)
37. A. Sikora, Z. Tuzar, Makromol. Chem. **184**, 2049 (1983)
38. C. Price, Pure Appl. Chem. **55**, 1563 (1983)
39. P. Linse, M. Malmsten, Macromolecules **25**, 5434 (1992)
40. N.K. Reddy, P.J. Fordham, D. Attwood, C. Booth, Chem. Soc., Faraday Trans. **86**, 1569 (1991)
41. G. Wanka, H. Hoffmann, W. Ulbricht, Macromolecules **27**, 4145 (1994)